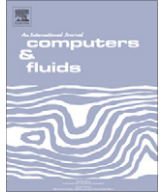




Contents lists available at ScienceDirect

Computers & Fluids

journal homepage: www.elsevier.com/locate/complfluid

Theoretical evaluation of the influence of geometric parameters and materials on the behavior of the airflow in a solar chimney

Cristiana B. Maia^{a,*}, André G. Ferreira^b, Ramón M. Valle^c, Márcio F.B. Cortez^c

^a Pontifícia Universidade Católica de Minas Gerais, Av. Dom José Gaspar, 500, Coração Eucarístico, Belo Horizonte, Minas Gerais, Brazil

^b Centro Federal de Educação Tecnológica de Minas Gerais, Av. Amazonas, 5253, Nova Suíça, Belo Horizonte, Minas Gerais, Brazil

^c Departamento de Engenharia Mecânica, Universidade Federal de Minas Gerais, Av. Antônio Carlos, 6627 – Campus Pampulha, Belo Horizonte, Minas Gerais, Brazil

ARTICLE INFO

Article history:

Received 11 July 2007

Received in revised form 29 May 2008

Accepted 10 June 2008

Available online xxx

ABSTRACT

An analytical and numerical study of the unsteady airflow inside a solar chimney was performed. The conservation and transport equations that describe the flow were modeled and solved numerically using the finite volumes technique in generalized coordinates. The numerical results were physically validated through comparison with the experimental data. The developed model was used for airflow simulation in solar chimneys with operational and geometric configurations different from those found in the experimental prototype. Analysis showed that the height and diameter of the tower are the most important physical variables for solar chimney design.

© 2008 Elsevier Ltd. All rights reserved.

1. Introduction

Solar chimneys are devices which use incident solar energy to generate hot airflow by, simply and efficiently combining three known technologies: solar collectors or covers, chimneys, and turbines [12]. The solar collector is a translucent disc, suspended over the ground and opened at its edges (Fig. 1). The tower of the system is placed in the center of the solar collector. A fraction of the solar radiation incident on the solar collector reaches the ground, increasing its temperature. The ground transfers heat, through convection, to the air under the solar collector. As air is heated, it moves up through buoyant forces towards the chimney. The hot air that leaves the tower is continually renewed by air, at ambient temperature, which enters through the solar collector edge. Flow energy can be converted into mechanical energy in one or more turbines placed at the base of the tower and into electric energy in conventional generators. The thermal energy of the flow can be used for other aims, such as ambient heating and drying of products in general, with the potential for significant uses in the drying of agricultural products.

Several studies about solar chimneys have been performed to numerically predict the airflow behavior inside the device. Bernardes et al. [3] developed a model to estimate power output of solar chimneys and to examine the effect of various ambient conditions and structural dimensions on the power output. Zhou et al. [16] built a pilot experimental solar chimney thermal power generating equipment in China. They carried out a simulation study to investigate the power generating system performance based on a devel-

oped mathematical model. Tingzhen et al. [14] presented a numerical simulation of the solar chimney power plant systems coupled with turbine. Mathur et al. [8] presented experimental investigations on solar chimney for room ventilation and Bassiouny and Koura [2] presented an analytical and numerical study of solar chimney use for room natural ventilation.

In 1968, Professor J. Schlaich proposed the solar chimney. In 1981, a pilot plant of 50 kW in Manzanares, Spain was constructed. The flow inside the solar chimney, with a height of 195 m, reached velocities of 12 m/s, with temperature increases of 17 °C above ambient temperature [11]. The equipment operated from 1982 to 1989, and was connected to the local electric network between 1986 and 1989 [15]. Economic assessments, based on the experience and knowledge acquired during the design and functioning of the Manzanares plant, showed that solar chimneys with power starting at 100 MW are able to generate energy at a cost similar to that from conventional plants [13]. It is estimated that solar chimneys with a height of 1000 m are able to generate 100 MW, with velocities of 16 m/s and temperature increases of 35 °C above the ambient temperature [11].

However, very high structures are needed for electric generation. Solar chimneys with smaller dimensions are feasible for drying, as they generate airflow with temperature and mass flow values within the minimum and maximum limits required for the adequate drying of most agricultural products [4,7]. The solar chimneys would have approximately the same dimensions as commercially disposable grain storage systems. A model able to predict the velocity and temperature of the flow can be a useful tool to help in the design of a solar chimney to dry agricultural products.

This paper presents a numerical analysis of the turbulent flow inside a solar chimney under an unsteady condition. The

* Corresponding author. Tel.: +55 31 99340042; fax: +55 31 3409 2252.
E-mail address: cbmaia@oi.com.br (C.B. Maia).

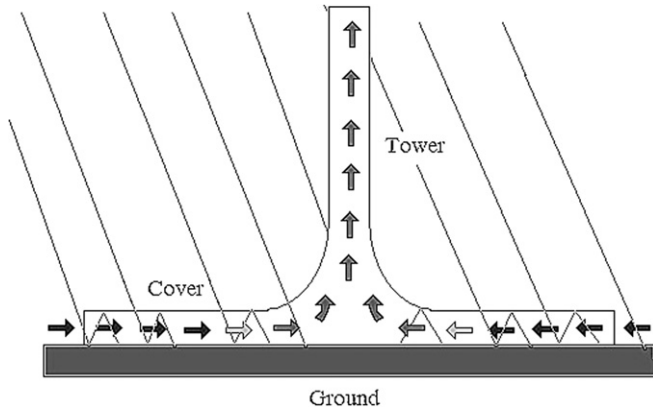


Fig. 1. Solar chimney operation.

mathematical model and the proposed numerical methodology were validated physically through the comparison of theoretical results using experimental data obtained from a prototype built specifically for this goal. Once validated, the developed model was applied in different conditions, allowing the evaluation of the influence of the main physical and operational variables in the flow behavior.

2. Mathematical model

The physical domain and the solution domain are shown in Fig. 2. The radius and the height of the tower are designated, respectively, by Rt and Ht . The cover radius is defined as Rc . At the cover entrance, the height is named $Hc2$, increasing linearly until it reaches the final height $Hc1$, and remains constant. The airflow is described using the cylindrical coordinate system, assuming that air is a Newtonian fluid and an ideal gas and assuming axi-symmetric hypothesis. The equations that describe the flow are given by Mass conservation:

$$\frac{\partial \rho}{\partial t} + \frac{\partial}{\partial x}(\rho u) + \frac{1}{r} \frac{\partial}{\partial r}(r \rho v) = 0. \quad (1)$$

Linear x -momentum conservation:

$$\begin{aligned} \frac{\partial}{\partial t}(\rho u) + \frac{\partial}{\partial x}(\rho u u) + \frac{1}{r} \frac{\partial}{\partial r}(r \rho u v) \\ = -\frac{\partial}{\partial x} \left(p + \frac{2}{3} \rho k \right) + \frac{\partial}{\partial x} \left(\mu_e \frac{\partial u}{\partial x} \right) + \frac{1}{r} \frac{\partial}{\partial r} \left(r \mu_e \frac{\partial u}{\partial r} \right) \\ + \frac{\partial}{\partial x} \left(\mu_e \frac{\partial u}{\partial x} \right) + \frac{1}{r} \frac{\partial}{\partial r} \left(r \mu_e \frac{\partial v}{\partial x} \right) + (\rho_o - \rho) g. \end{aligned} \quad (2)$$

Linear r -momentum conservation:

$$\begin{aligned} \frac{\partial}{\partial t}(\rho v) + \frac{\partial}{\partial x}(\rho u v) + \frac{1}{r} \frac{\partial}{\partial r}(r \rho v v) \\ = -\frac{\partial}{\partial r} \left(p + \frac{2}{3} \rho k \right) + \frac{\partial}{\partial x} \left(\mu_e \frac{\partial v}{\partial x} \right) + \frac{1}{r} \frac{\partial}{\partial r} \left(r \mu_e \frac{\partial v}{\partial r} \right) \\ + \frac{\partial}{\partial x} \left(\mu_e \frac{\partial u}{\partial r} \right) + \frac{1}{r} \frac{\partial}{\partial r} \left(r \mu_e \frac{\partial v}{\partial r} \right) - 2 \mu_e \frac{v}{r^2}. \end{aligned} \quad (3)$$

Energy conservation:

$$\begin{aligned} \frac{\partial}{\partial t}(\rho T) + \frac{\partial}{\partial x}(\rho u T) + \frac{1}{r} \frac{\partial}{\partial r}(r \rho v T) \\ = \frac{\partial}{\partial x} \left[\left(\frac{\mu}{Pr} + \frac{\mu_t}{Pr_t} \right) \frac{\partial T}{\partial x} \right] + \frac{1}{r} \frac{\partial}{\partial r} \left[r \left(\frac{\mu}{Pr} + \frac{\mu_t}{Pr_t} \right) \frac{\partial T}{\partial r} \right] \\ + \frac{\beta T}{c_p} \left[\frac{\partial \rho}{\partial t} + \frac{\partial}{\partial x}(\rho u) + \frac{1}{r} \frac{\partial}{\partial r}(r \rho v) - \rho \frac{\partial u}{\partial x} - \frac{\rho}{r} \frac{\partial}{\partial r}(r v) \right]. \end{aligned} \quad (4)$$

In which ρ_o is the reference fluid density and μ_e is the effective viscosity, defined as the sum of the eddy viscosity μ_t and the fluid dynamic viscosity μ .

In order to solve the previous equations, it is necessary to determine the eddy viscosity μ_t . In this study, the standard κ - ε model of Launder and Spalding [6] with wall functions was used. In this model, the eddy viscosity μ_t is evaluated from the turbulent kinetic energy κ and the dissipation of the turbulent kinetic energy ε :

$$\mu_t = \rho C_\mu C_D \frac{\kappa^2}{\varepsilon}. \quad (5)$$

Transport equations for the turbulent variables added are needed to evaluate the eddy viscosity, as shown below. Turbulent kinetic energy conservation:

$$\begin{aligned} \frac{\partial}{\partial t}(\rho \kappa) + \frac{\partial}{\partial x}(\rho u \kappa) + \frac{1}{r} \frac{\partial}{\partial r}(r \rho v \kappa) \\ = \frac{\partial}{\partial x} \left(\frac{\mu_e}{\sigma_\kappa} \frac{\partial \kappa}{\partial x} \right) + \frac{1}{r} \frac{\partial}{\partial r} \left(r \frac{\mu_e}{\sigma_\kappa} \frac{\partial \kappa}{\partial r} \right) + P_\kappa + G_\kappa - \rho C_d \varepsilon. \end{aligned} \quad (6)$$

Dissipation of turbulent kinetic energy:

$$\begin{aligned} \frac{\partial}{\partial t}(\rho \varepsilon) + \frac{\partial}{\partial x}(\rho u \varepsilon) + \frac{1}{r} \frac{\partial}{\partial r}(r \rho v \varepsilon) \\ = \frac{\partial}{\partial x} \left(\frac{\mu_e}{\sigma_\varepsilon} \frac{\partial \varepsilon}{\partial x} \right) + \frac{1}{r} \frac{\partial}{\partial r} \left(r \frac{\mu_e}{\sigma_\varepsilon} \frac{\partial \varepsilon}{\partial r} \right) + \frac{C_{1\varepsilon}}{\kappa} (P_\kappa + G_\kappa) (1 + 0.8 R_f) - C_{2\rho} \frac{\varepsilon^2}{\kappa}. \end{aligned} \quad (7)$$

In which P_κ represents the turbulent kinetic energy source term, defined by

$$P_\kappa = \mu_t \left[\left(\frac{\partial u}{\partial r} + \frac{\partial v}{\partial x} \right)^2 + 2 \left(\frac{\partial u}{\partial x} \right)^2 + 2 \left(\frac{\partial v}{\partial r} \right)^2 + 2 \left(\frac{v}{r} \right)^2 \right]. \quad (8)$$

Terms that take into account the buoyant force in the flow, described by Rodi [10], were added to the turbulent variables transport equations.

The term G_κ represents the turbulent kinetic energy production caused by buoyant force effects, given by

$$G_\kappa = -\frac{\beta g}{\rho} \frac{\mu_t}{Pr_t} \frac{\partial T}{\partial x} \quad (9)$$

and R_f is the Richardson number, defined as the ratio between the turbulent kinetic energy production due to the buoyant force effect (G_κ) and the total production of turbulent kinetic energy ($G_\kappa + P_\kappa$).

The constants of the adopted turbulence model are given on Table 1.

The boundary conditions used are shown in Fig. 3. At the tower outlet, the flow is assumed to be fully developed. At the center of the device, axi-symmetric conditions were adopted.

At the walls, no-slip and impermeable boundary conditions were used. These conditions were applied at the cover, the joint, the tower walls, and the ground surface.

At the cover entrance, the velocity was prescribed. In the axial direction (u), the velocity was assumed to be zero. However, since the flow is generated by buoyant forces, the velocity in the radial direction (v) is unknown. Therefore, the radial velocity is determined using a mass balance to each step, until the convergence of the results.

Air at unsteady ambient temperature enters the cover. Insulation conditions were adopted for the tower walls and the joint area. The ground surface temperature was determined by an energy balance based on measured solar radiation values. This temperature is time dependent, characterizing the unsteady flow condition. At the cover region, an energy balance was made between the air inside and outside the system.

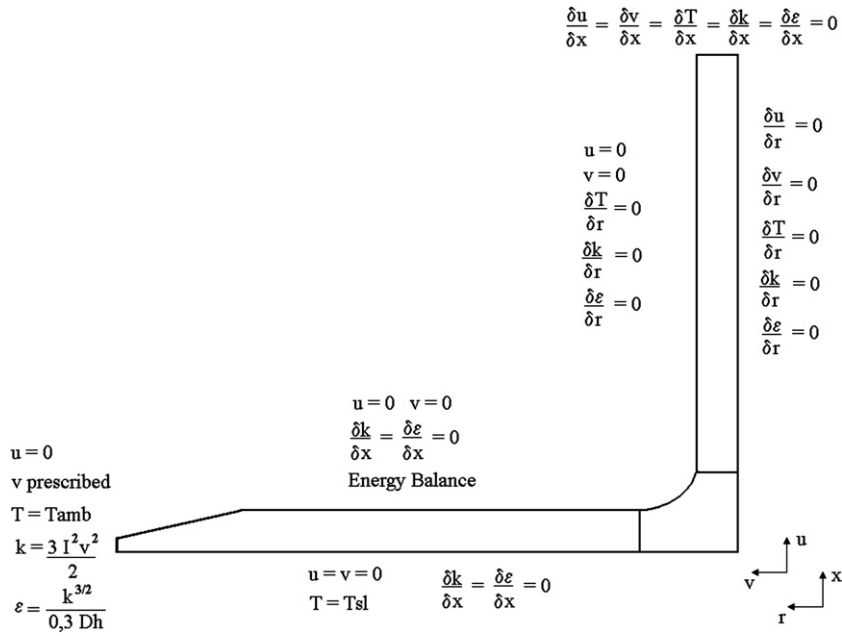


Fig. 3. Boundary conditions.

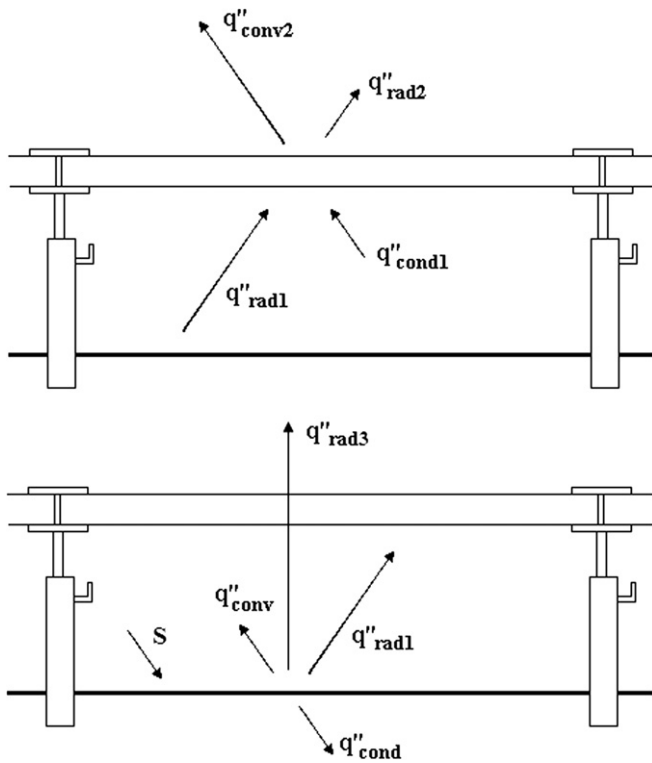


Fig. 4. Heat flux balance at the cover and at the ground.

where κ , ρ and C_p , are, respectively, the thermal conductivity, the density and the specific heat of the ground.

3. Experimental prototype and numerical methodology validation

A physical prototype was built for the validation of the mathematical model and the numerical methodology used. The prototype consists of a tower with a height (Ht) of 12.3 m and a radius

(Rt) of 1 m and a cover with a radius (Rc) of 12.5 m and a variable height (Hc) of between 5 cm in the inlet to 50 cm in the joint (Figs. 5 and 6). For the numerical simulation, 376 control volumes were used in the main flow direction, whereas 32 control volumes were used in the direction normal to the main flow. The timestep used was 5 min. Both time and space grids were defined based on grid tests. The flow was simulated for July 7th. The results are presented for a 24-h period and, for the instantaneous analysis, the time of simulation was 1:00 pm.

Fig. 7 presents the velocity profile for a transversal section of the tower. Small differences between the numerical and experimental values can be seen, explained either by numerical errors or by experimental uncertainties. Nevertheless, the maximum differences (around 2%) are below the potential error value for the anemometers used.

Fig. 8 presents the temperature profile at a transversal section of the tower correspondent to 90% of the tower's height ($x/Ht = 0.9$). The numerical and experimental values were close, with maximum differences of approximately 1.0 °C. It can be noticed that the inlet air temperature, at this time, was 30 °C. Fig. 9 presents the temperature profile on the cover, for the non-dimensional radius of $r/Rc = 0.15$. Additional information on the experimental data used to validate the numerical results can be seen on Ferreira et al. [4] and Maia et al. [7].

4. Results and discussion

Based on the dimensions of the built physical prototype and on the results of the computational simulation (validated through experimental data), the influence of the main geometric parameters of the solar chimney on the behavior of the airflow was assessed. The geometric parameters analyzed were the radius and the height of the tower, and the radius and the final height of the cover.

4.1. Influence of the tower radius

Fig. 10 illustrates the mass flow as function of time, for three different values of the tower radius. It can be observed that an increase in the tower radius produces an increase in the mass flow.



Fig. 5. Experimental prototype.

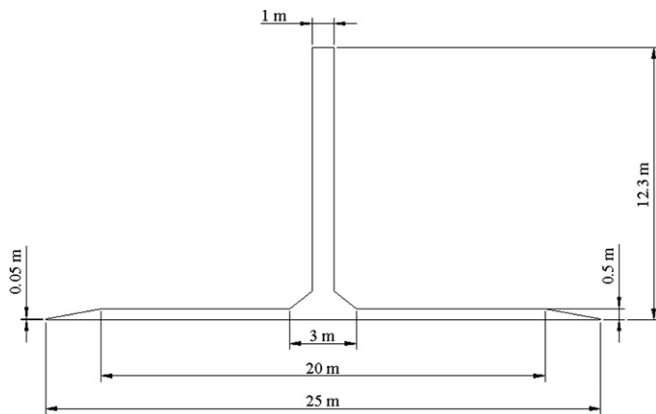


Fig. 6. Dimensions of the prototype.

However, due to the increase in the flow area, the velocity decreases in the center of the tower (Fig. 11).

When the cover parameters are fixed and the radius of the tower is increased, the mass flow increases, resulting in an increase of the velocity in the entire system. Fig. 12 shows the development of the velocity in the cover for the three analyzed tower radius values. It can be observed that the flow temperature increases towards the center of the solar chimney, due to the heat exchanges between the ground and the airflow. Close to the center of the solar chimney, due to the reduction of the flow area, the velocity of the airflow decreases and the temperature starts to rise again. An increase on the tower radius increases the mass flow. Then, a larger volume of air needs to be heated in the cover during the same period of time, causing the flow temperature in the cover to decrease. Fig. 13 shows the temperature along the cover for the analyzed tower radius values. The larger the tower radius, the lower the temperature of the flow in the cover.

The increase in the mass flow caused by the increase on the tower radius also results in the reduction of the average temperature of the flow in the tower, as shown in Fig. 14. It can be noted that the flow temperature in the tower is always greater than the ambient temperature outside the solar chimney.

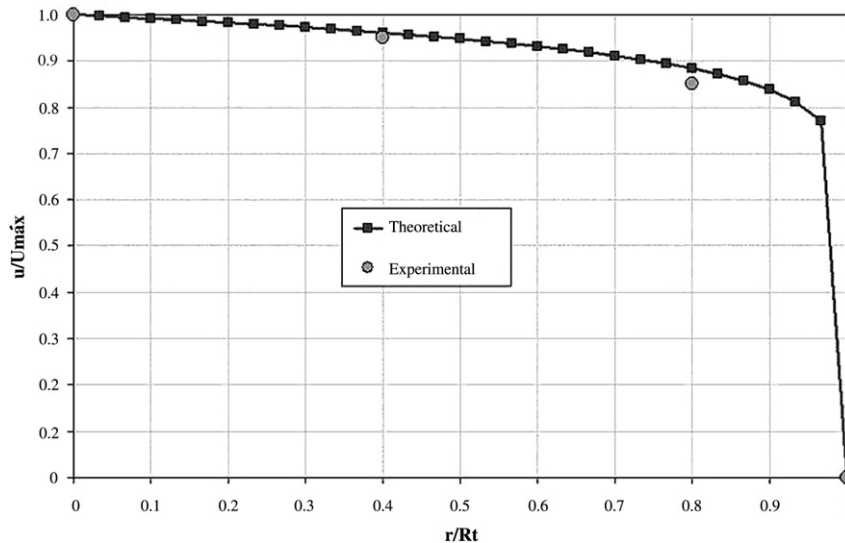


Fig. 7. Dimensionless velocity profile in a tower section (theoretical and experimental).

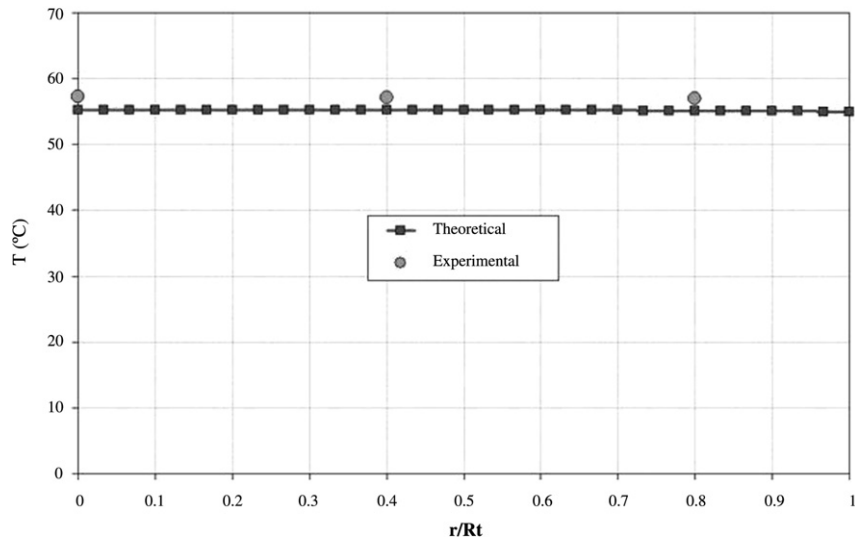


Fig. 8. Temperatures in the tower.

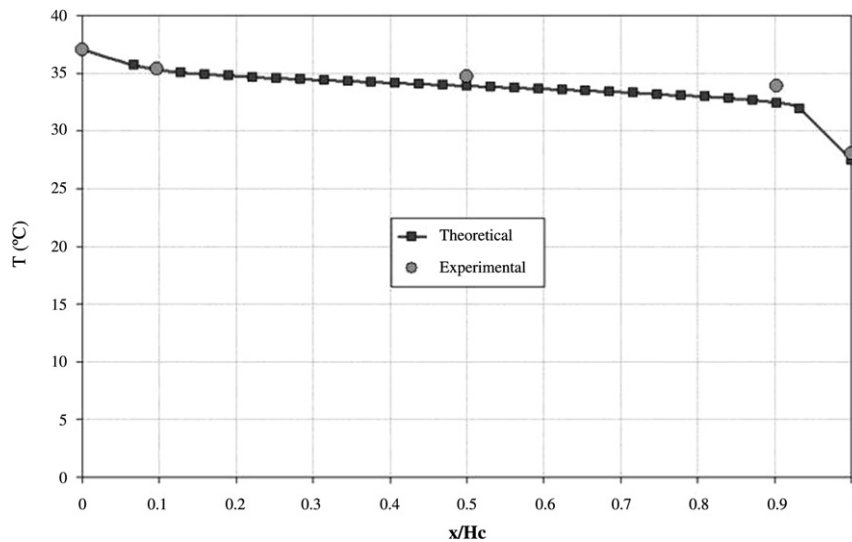


Fig. 9. Temperatures in the cover.

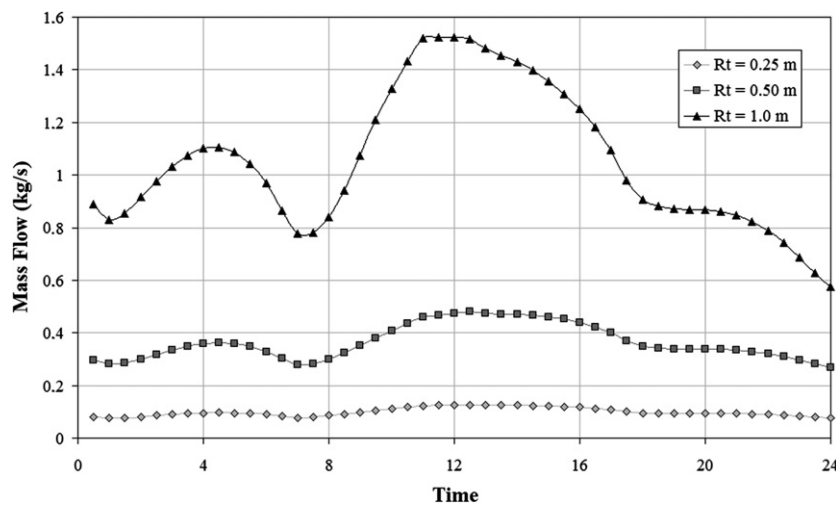


Fig. 10. Influence of the tower radius on the mass flow.

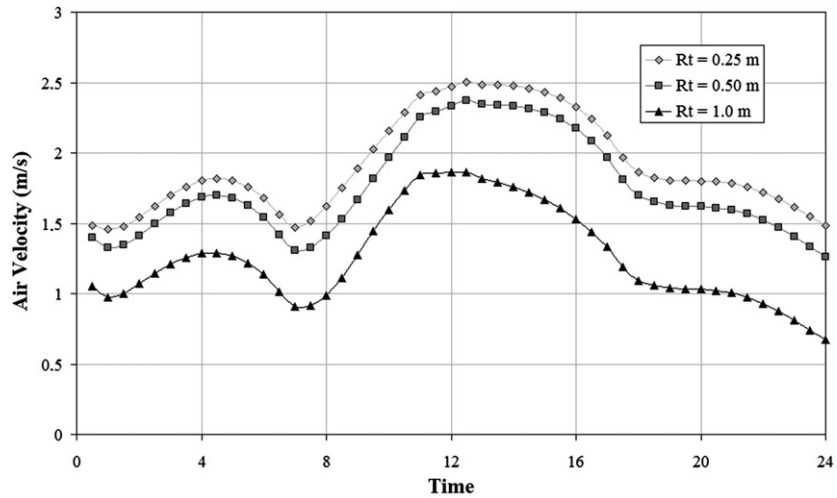


Fig. 11. Influence of the tower radius on the velocity of the tower symmetry axis.

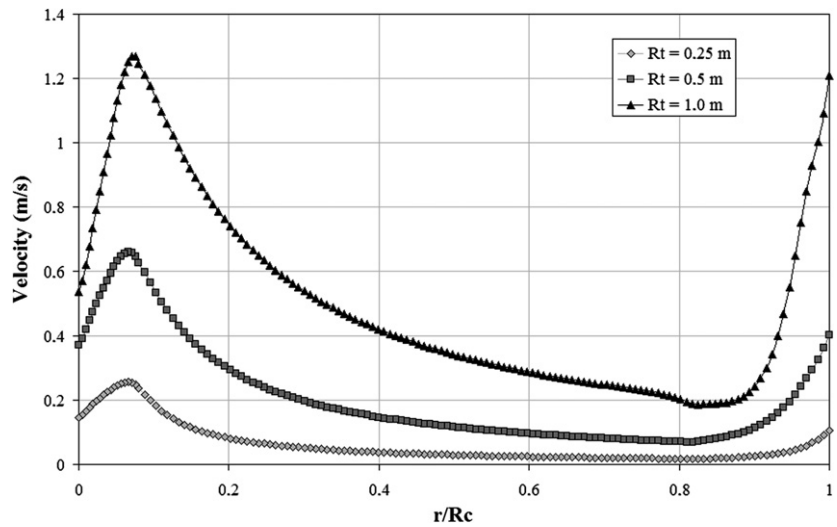


Fig. 12. Influence of the tower radius on the development of the velocity along the cover.

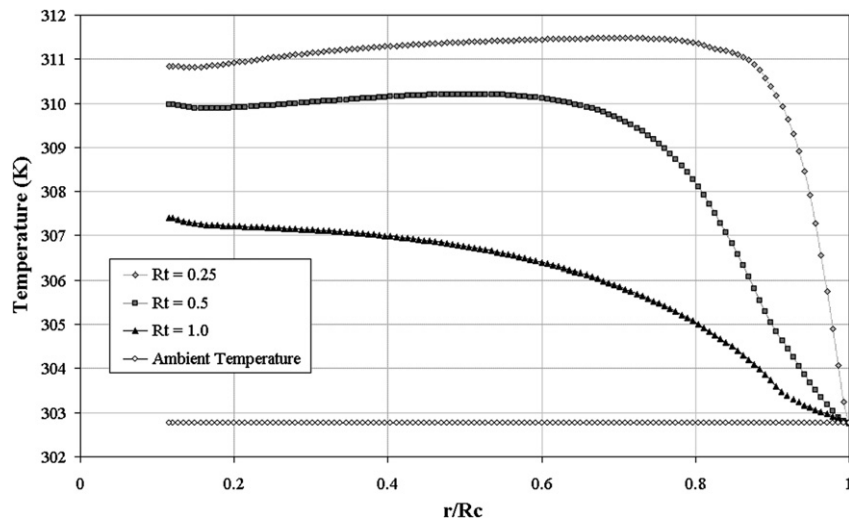


Fig. 13. Influence of the tower radius on the development of the temperature along the cover.

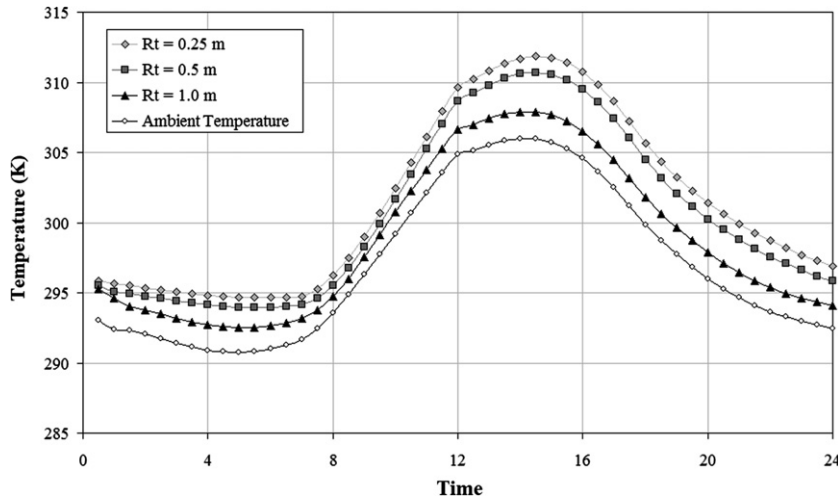


Fig. 14. Influence of the tower radius on the flow average temperature in the tower.

4.2. Influence of the tower height

The computational program was simulated for tower heights of 10 m, 12.3 m (corresponding to the height of the prototype), 20 m, 30 m, and 50 m. The analysis showed that an increase in the height of the tower causes an increase in the pressure drop along the tower, resulting in greater the mass flow values and higher flow velocities. Fig. 15 shows the air velocity at the center of the tower, as a function of the time, for the analyzed height values.

As observed, larger mass flows and velocities cause a reduction in the temperature values. Fig. 16 presents the average flow temperature at the tower outlet, as a function of time.

4.3. Influence of the cover radius

The influence of the cover radius on the behavior of the flow was evaluated through the simulation of the computational program for values of 4 m, 8 m, 12.5 m, and 20 m, maintaining the other parameters at the dimensions of the prototype. The average flow temperature at the tower outlet is shown in Fig. 17, as a function of time.

It can be observed that an increase in the cover radius causes the tower temperature to increase. However, this phenomenon oc-

curs only until the tower radius reaches 12.5 m. Above this value, the tower temperature remains constant. Fig. 18 illustrates the development of the velocity in the cover for the analyzed cover radius. The cover inlet corresponds to $r/Rc = 1$. Near the cover inlet, due to the increase of the cover height, there is an increase in the cross-section of the flow, causing a decrease in the flow velocity. When the height of the cover reaches its maximum value, the cross-section begins to decrease with the reduction of the radius, increasing the flow velocity. The maximum value of the velocity is achieved at the junction of the tower and the cover. The flow area increases while the velocity decreases until the flow reaches the tower ($r/Rc = 0$).

Fig. 19 shows the development of the temperature in the cover. The air enters the cover at ambient temperature. As the air flows towards the tower, its temperature increases. For the cover radii of 4 m and 8 m, the flow temperature increases along the cover. However, for larger values of the radius, at a certain point, due to the increase in the velocity, the temperature begins to drop. The increase in the temperature at the joint is explained by the reduction in the velocity and by adiabatic conditions imposed by the boundary conditions. The temperature at the end of the cover remains approximately constant for the radius of 12.5 m and 20 m.

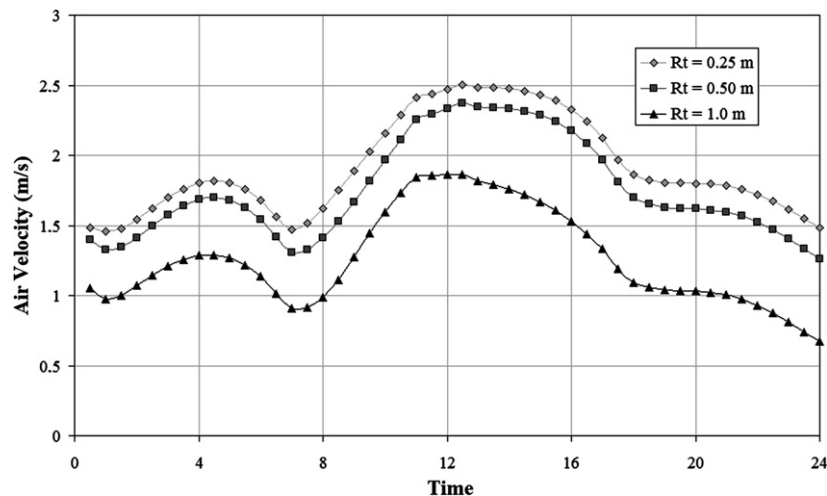


Fig. 15. Influence of the tower radius on the velocity of the tower symmetry axis.

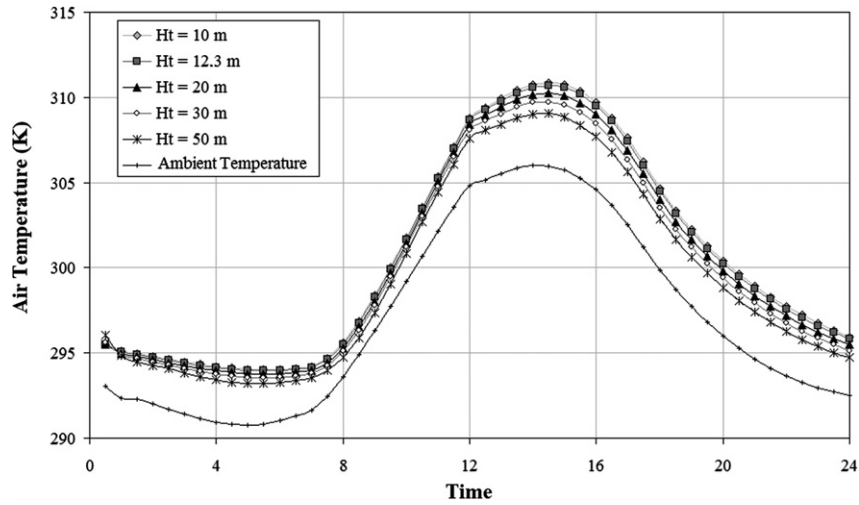


Fig. 16. Influence of the tower height on the average temperature in the tower.

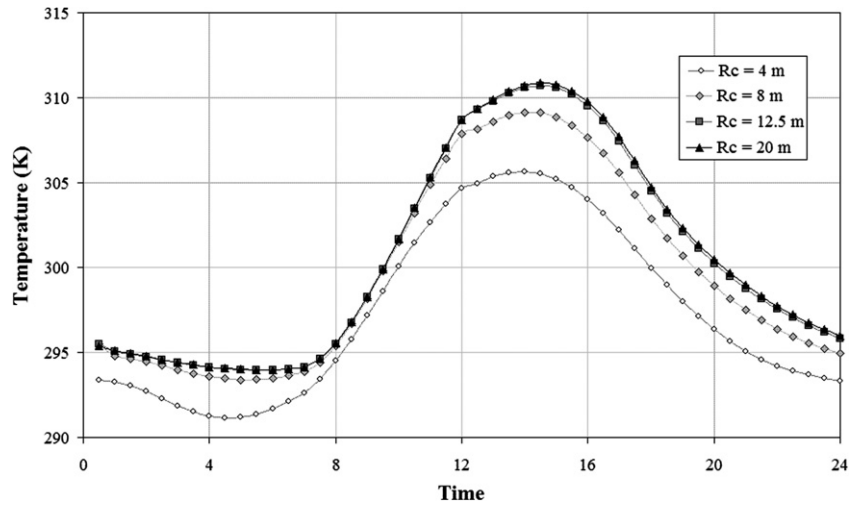


Fig. 17. Influence of the cover radius on the average temperature in the tower.

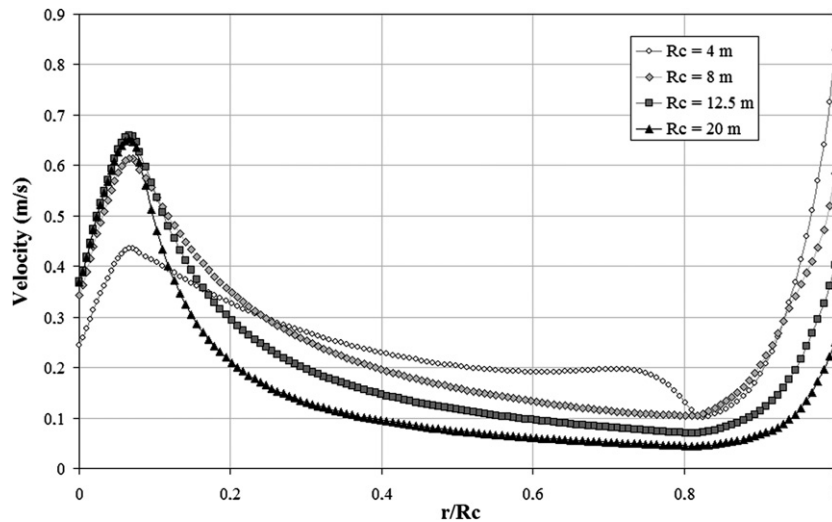


Fig. 18. Influence of the cover radius on the development of the velocity along the cover.

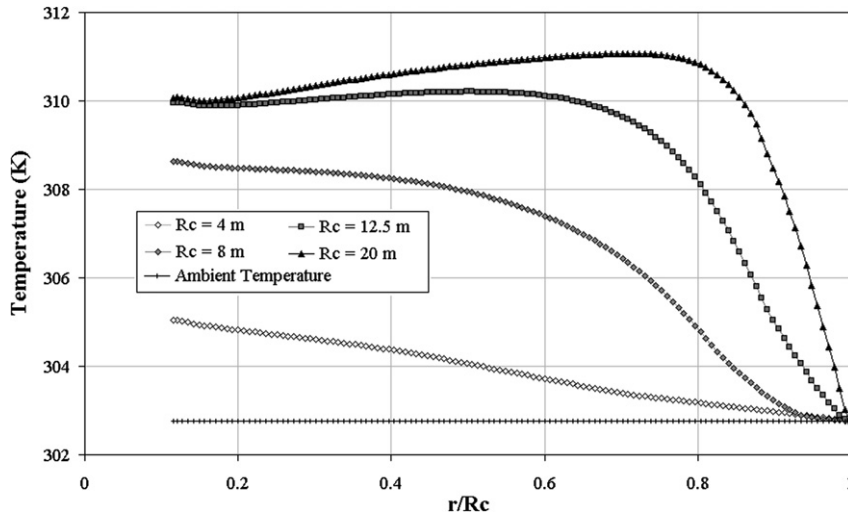


Fig. 19. Influence of the cover radius on the development of the temperature along the cover.

4.4. Influence of the cover height

The computational program was simulated for the cover heights of 0.25 m, 0.50 m, and 1 m. An increase in the cover height causes a reduction in the heat loss of the flow in the cover, allowing the mass flow to achieve higher values. Fig. 20 represents the mass flow as a function of the time, for the analyzed cover heights.

Although the increase in the cover height causes an increase in the flow, the velocity of the flow in the cover is reduced due to an increase in the cross-section (Fig. 21). The reduction in the velocity results in an increase in the time required by the flow to cross the cover, intensifying the heat exchanges between the ground and the air, causing a small rise in the flow temperature. Fig. 22 shows the average temperature of flow at the tower outlet as a function of the time.

An assessment of the influence of the height cover in the solar chimney inlet ($Hc2$) was also performed. Numerical results did not show significant differences for the heights of 0.05 m, 0.25 m, and 0.50 m. However, the experience gained on the tests indicates that the cover height at the entrance must be as low as possible, to prevent side winds from entering the chimney, thus removing the heated air in the cover.

A theoretical evaluation of the flow behavior was performed to analyze the influence of the cover material. The computational program was simulated using three common materials used in solar devices: a thermal diffuser plastic film (used in the prototype), a plastic film used in greenhouses, and glass. Experimental tests indicate that the thermal diffuser has an average transmittance to solar radiation of $(72 \pm 5)\%$ and an average transmittance to infrared of $(40.0 \pm 1.5)\%$ [5]. Glass has a transmittance to solar radiation of approximately 92% and to infrared lower than 5%. The plastic film for greenhouses has an average transmittance of $(84 \pm 6)\%$ to solar radiation and an average transmittance of $(67.0 \pm 0.7)\%$ to the infrared (Ferreira, 2004). Fig. 23 shows the numerical results of the ground temperature under the cover during the day. It can be observed that when the materials with higher transmittances to solar radiation are used, the ground temperatures are higher, resulting in higher flow temperatures.

Fig. 24 shows the flow velocity in the center of the tower. When glass is used, the flow temperatures are higher, as observed in Fig. 23. Since the flow is generated by buoyant forces created by differences in the temperature of the flow, higher velocities are reached.

The definition of the most suitable material for the cover can only be done after an analysis of the financial and the operational

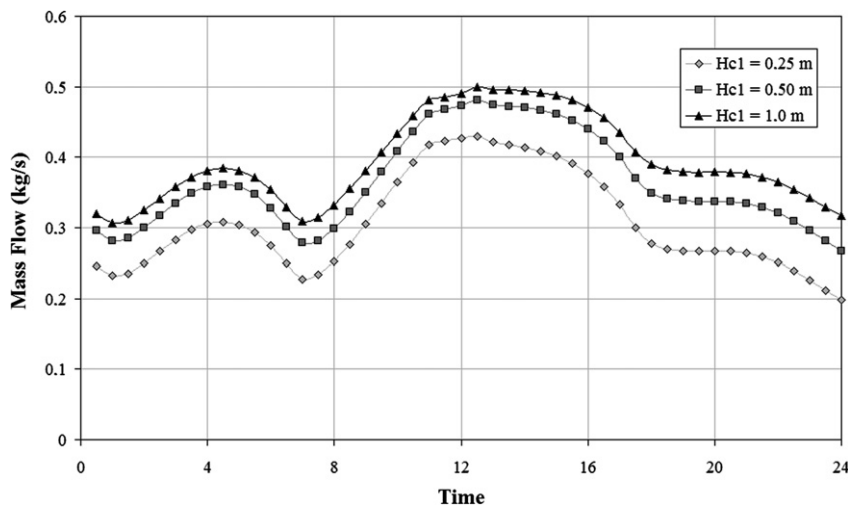


Fig. 20. Influence of the cover height on the development of the mass flow.

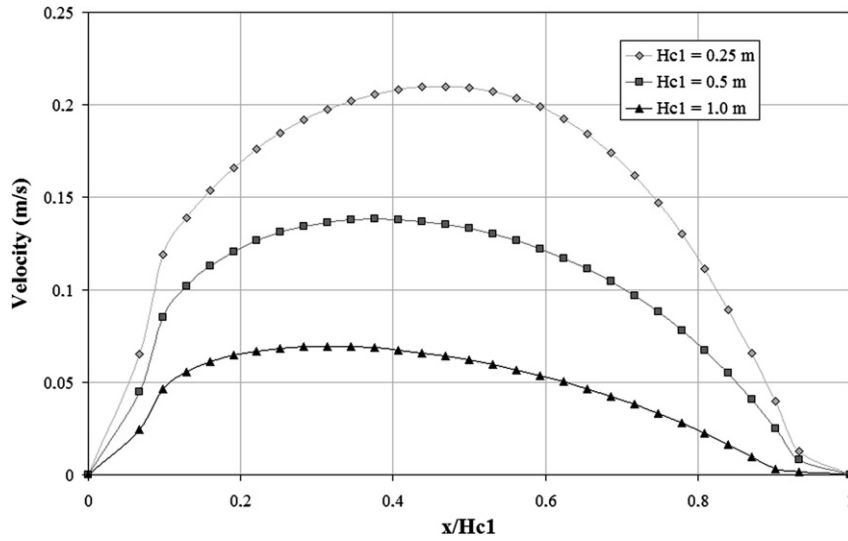


Fig. 21. Influence of the cover height on the velocity in the cover.

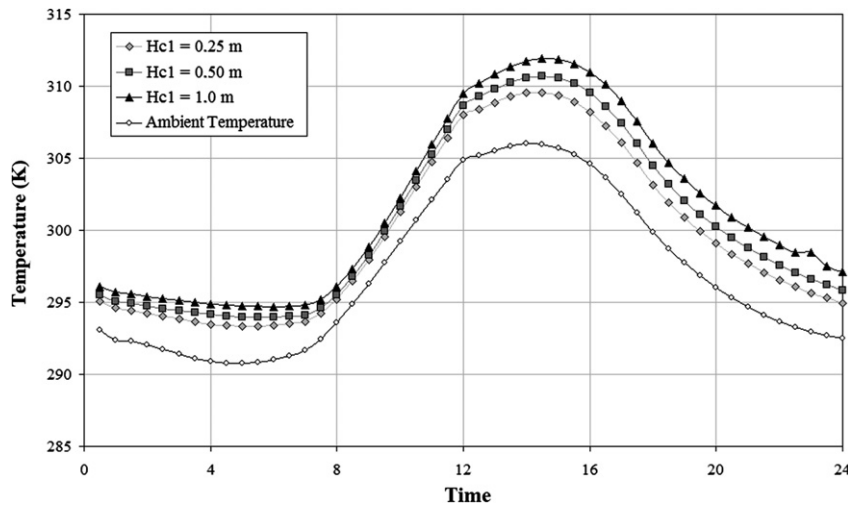


Fig. 22. Influence of the cover height in the average temperature in the tower.

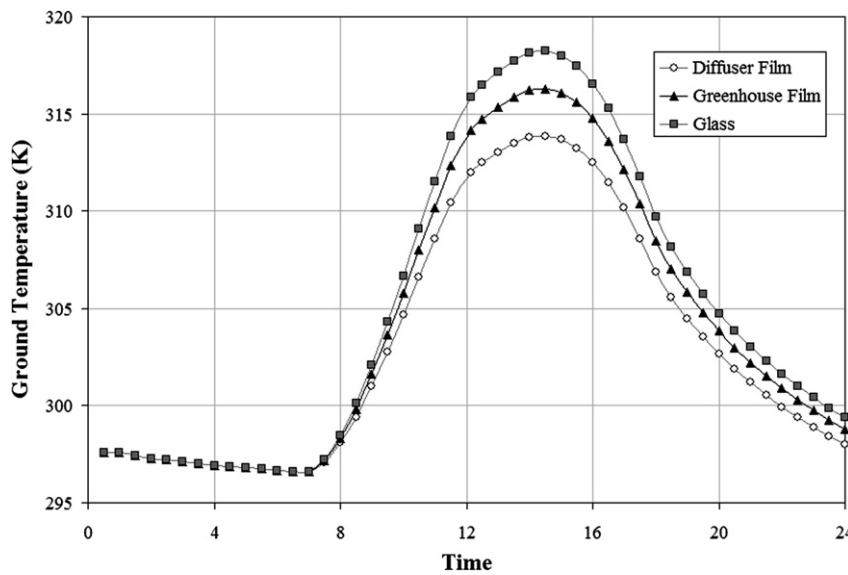


Fig. 23. Influence of the cover material on the ground temperature.

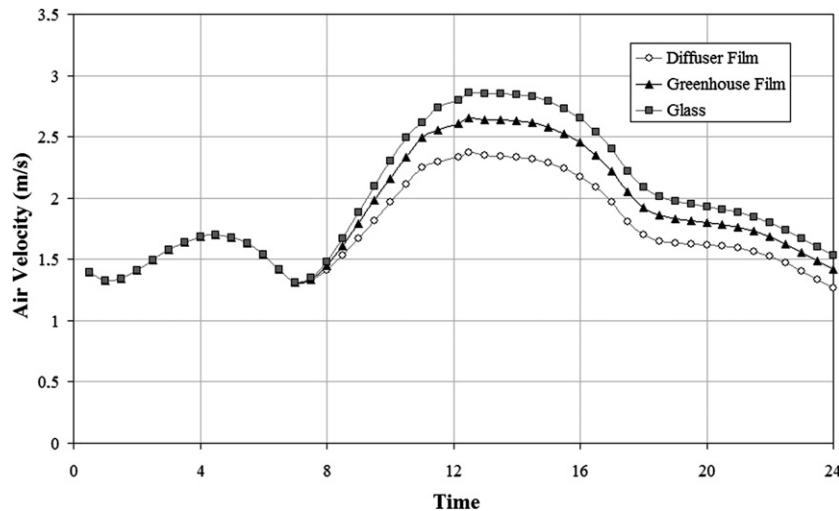


Fig. 24. Influence of the cover material on the velocity in the tower.

aspects. Although glass provides higher temperature and velocity values, it is more expensive, more fragile, and heavier. The greenhouse film has higher transmittance to solar radiation than the thermal diffuser film (allowing a higher value of solar radiation to reach the ground); however, its infrared transmittance is higher than the infrared transmittance of the glass and of the thermal diffuser. Therefore, the thermal losses from the ground to the cover and to the ambient are higher. Moreover, experimental tests indicated that its mechanical resistance is lower than the resistance of the thermal diffuser plastic film.

5. Conclusions

A theoretical analysis of the turbulent flow inside a solar chimney was presented. Flow was modeled through the numeric solution of the conservation equations of mass, energy, and momentum, as well as the turbulent variables transport equations. Results were validated experimentally through their comparison with the experimental data obtained by means of a physical prototype. It was observed that the most important physical variables in a solar chimney project are the tower dimensions, as they cause the most significant variations in the flow behavior. An increase in the height and diameter of the tower produces an increase in the mass flow and a decrease in the flow temperature. The physical properties of the materials used in the solar chimney define the flow characteristics. However, the selection of these materials must also include technical, financial, and operational criteria.

The development of a model of the airflow allows one to determine the fields of velocity and temperature inside solar chimneys regardless of its dimensions, thus making it possible to evaluate the influence of physical dimensions and operational variables on

the flow behavior. The developed model is a helpful tool in the design and operation of solar chimneys, allowing the determination of the most suitable parameters in different conditions.

References

- [1] AEA technology engineering software limited. CFX – TASCFlow user documentation, version 5.5, Waterloo, Canada. 2001.
- [2] Bassiouny R, Koura NSA. An analytical and numerical study of solar chimney use for room natural ventilation. *Energ Buildings* 2008;40:865–73.
- [3] Bernardes MA dos S, Voß A, Weinrebe G. Thermal and technical analyses of solar chimneys. *Sol Energy* 2003;75:511–24.
- [4] Ferreira AG, Maia CB, Cortez MFB, Valle RM. Technical feasibility assessment of a solar chimney for food drying. *Sol Energy* 2008;82:198–205.
- [5] Ferreira AG, Maia CB, Valle RM, Cortez MFB. Balanço Energético de uma Chaminé Solar. *Ciência & Engenharia* 2006;15:37–43.
- [6] Launder BE, Spalding DB. The numerical computation of turbulent flows. *Comput Methods Appl Mech* 1974;3:269–89.
- [7] Maia CB, Ferreira AG, Valle RM, Cortez MFB. Analysis of the airflow in a prototype of a solar chimney dryer. *Heat Transfer Eng*, 2009, 30, in press.
- [8] Mathur J, Bansal NK, Mathur S, Jain M. Anupma. Experimental investigations on solar chimney for room ventilation. *Sol Energy*, 80, 927–35.
- [9] Özisik MN. Heat conduction. 2nd ed. John Wiley & Sons; 1993.
- [10] Rodi W. Turbulence models and their application in hydraulics – a state of art review, IAHR, 3rd ed., Rotterdam: A.A. Balkema. 2001.
- [11] Schlaich J. The solar chimney, 14p. Available on: <http://www.sbp.de>. 2002.
- [12] Schlaich J. The solar chimney, electricity from the Sun, Edition Axel Menges, Stuttgart, 59p. 1995.
- [13] Schlaich J, Schiel W. Solar chimneys, encyclopedia of physical science and technology, 3rd ed., 2000.
- [14] Tingzhena M, Weia L, Guolinga X, Yanbina X, Xuhua G, Yuanb P. Numerical simulation of the solar chimney power plant systems coupled with turbine. *Renew Energy* 2008;33:897–905.
- [15] Trieb F, Langniß O, Klaiß H. Solar electricity generation – a comparative view of technologies, costs and environmental impact. *Sol Energy* 1997;59(1–3): 89–99.
- [16] Zhou X, Yang J, Xiao Bo, Hou G. Simulation of a pilot solar chimney thermal power generating equipment. *Renew Energy* 2007;32(10):1637–44.